Hindawi
Journal of Robotics
Volume 2022, Article ID 2365006, 13 pages
https://doi.org/10.1155/2022/2365006

Research Article

Unmanned Aerial Vehicle Surveying and Mapping Trajectory Scheduling and Autonomous Control for Landslide Monitoring

Shifang Liao,[1] Manzhu Ye,[2] Rongcai Yuan,[3] and Wanzhi Ma[4]

[1]*School of Resource & Environment and Historical Culture, Xianyang Normal University, Xianyang, Shaanxi 712000, China*
[2]*School of Surveying & Testing, Shaanxi Railway Institute, Weinan, Shaanxi 714000, China*
[3]*Xi'an Zhongke Xingyun Space Information Research Institute Co., Ltd.,, Xi'an, Shannxi 710000, China*
[4]*School of Educational Science, Ningxia Normal University, Guyuan, Ningxia 756000, China*

Correspondence should be addressed to Wanzhi Ma; mawanzhi79@nxnu.edu.cn

Received 29 December 2021; Revised 8 February 2022; Accepted 9 February 2022; Published 24 March 2022

Academic Editor: Shan Zhong

Real-time and efficient monitoring of geological disasters has received extensive attention in the application of UAV surveying and mapping control technology. The application of traditional landslide monitoring methods lacks the accuracy of control algorithms, which has become a hot issue currently facing. Based on the landslide surface subsidence monitoring method, this article designs the UAV trajectory scheduling subsidence monitoring software, which can monitor the UAV's flight status and navigation information, and draw the flight trajectory in real time. At the same time, the model solves the problem of storage and management of landslide inspection results by the landslide inspection management system, and realizes the functions of entering and querying landslide information, viewing inspection results, landslide safety judgment, generating reports, and autonomous control. The simulation results show that the global accuracy reaches 0.975, and the algorithm recognition degree reaches 99.8%, which promotes the reliability of the landslide monitoring data for the identification of the surveying and mapping trajectory, and provides a decision-making basis for landslide treatment.

1. Introduction

Due to the subsidence and deformation of the ground surface caused by landslide activities, the methods of subsidence monitoring have undergone a long-term process, ranging from traditional leveling traverse measurement and GPS monitoring to the more commonly used three-dimensional laser scanning monitoring and D-InSAR monitoring. These monitoring methods range from full-field to few-field measurements, and the observation efficiency is greatly improved, but their monitoring range, accuracy, and efficiency still cannot meet the needs of comprehensive monitoring of regional subsidence [1]. The emergence of UAV low-altitude photogrammetry at this stage has greatly improved the efficiency of monitoring with its high mobility and real-time performance. Its high-precision digital results are applied to various monitoring fields, including monitoring of mountain landslides, mudslides, and collapses. The terrain conditions of highway construction in mountainous areas are complex and changeable. Due to the consideration of many aspects, highway construction cannot avoid the use of high filling and deep excavation methods, which will form a high landslide structure, because such high landslides are all reconstructed from the original landform. Breaking the original balance relationship and balance conditions of the landform, the stress field will change accordingly, and the open-air slope will have cracks and landslide settlement and sliding due to the local lithology and structure, surface water, ground runoff, etc. [2–5].

At present, with the continuous development and progress of drone technology, autonomous drone navigation technology has gradually been applied to all walks of life in society, providing it with high-performance technology services such as safety, convenience, intelligence, and environmental protection, making people's life and social production have become more and more convenient and efficient [6–8]. The research and development of UAV autonomous navigation technology will continue to promote the innovation of social science and technology, which is of great significance to

the future development. With the vigorous development of national highway traffic, highway mileage has increased year by year. In the road operation stage, road maintenance and management are particularly important, and landslide inspection is a basic but important task in road maintenance and management. Daily regular inspections are conducive to real-time grasp of the stability and safety of landslides. Timely early warning and treatment of diseases are essential. At present, landslide inspections use manual inspections, generally using visual inspection, tapping, and touching. The terrain conditions of landslides are complex and changeable. When inspectors face high landslides and mountain landslides, manual inspections are very dangerous or even to reach certain areas of the landslide, resulting in inspection results that cannot fully reflect the true situation of the landslide. Therefore, conducting drone inspections for landslide disease has important practical significance for disaster reduction and prevention and traffic safety. In traditional manual inspection, visual inspection is the main method. Therefore, the operation mode of drones is used to replace or assist traditional inspection personnel's short-distance visual inspection, which makes landslide safety inspection possible [9–11].

UAV low-altitude photogrammetry as a fast, convenient, and safe image acquisition technology has been studied in the field of geological disaster investigation and other fields. The purpose of this article is to study the technical methods of using drones for landslide inspection to replace or assist manual road inspections, so as to ensure the safety of inspectors. According to the relevant requirements of the landslide inspection, starting from the actual inspection work, two technical methods of overall inspection and fine inspection of landslides based on unmanned low-altitude photogrammetry are proposed. In order to realize the early deformation recognition of the landslide in the area, this article uses drone photogrammetry technology to take multiple phases of the landslide to study its accuracy and deformation recognition methods. First, the image of the survey area is obtained by flying the drone, and then, the image is processed to obtain the point cloud data. Through continuous improvement of the number and location of ground control points, the accuracy of UAV aerial photography technology has been improved, and the accuracy has been increased from the decimeter level to the centimeter level. Before entering the test in the subsidence area, the UAV aerial survey plan was designed. Combining two more classic sparse and dense deployment schemes, the accuracy of the UAV digital results under the two schemes is verified to obtain a set of reasonable image control point schemes. The two sets of data, respectively cite the post difference technology to verify the digital results and verify the accuracy and superiority of the post difference technology. Under the same scheme, the DEM accuracy of tilt and vertical photography was compared, and the best tilt aerial photography plan was obtained.

2. Related Work

Compared with traditional methods of monitoring the regional surface, the rapid development of drone aerial photogrammetry technology in recent years has become more and more widely used. The drone technology is highly maneuverable, flexible, and lightweight in the process of acquiring images. The acquired images have high resolution and play an important role in surveying and mapping geographic information, earthquake mitigation and disaster relief, agricultural production estimation, water conservancy and hydropower, and transportation and construction. The most widely used technology in UAV photogrammetry technology is tilt photogrammetry technology. This technology has become one of the current research hotspots. With its high precision, high mobility, and high efficiency, it is suitable for operation in a variety of complex environments. [12–15].

At present, there are three methods for differential interferometry, namely, the two-track method of two InSAR images, the three-track method of three InSAR images, and the four-track method of four InSAR images. The deformation result measured by InSAR technology is the estimated value of the spatial average change in a certain area. This method makes up for the shortcomings of traditional monitoring methods for the sparse measurement points. It has the characteristics and advantages of large area, real time, and high precision, which effectively complements traditional monitoring. Zanol et al. [16] used the X-band and L-band of D-InSAR to monitor the subsidence of the central area of Utah. The results show that the L-band can accurately monitor the subsidence value of this area, and it is less affected by slope changes. Although it is difficult to achieve a high-precision level for subsidence monitoring using X-band, it can also monitor the survey area with a reasonable and accurate subsidence range. Figueiredo et al. [17] used high-resolution images to extract and monitor tunnel cracks to provide a solid guarantee for the safe operation of the subway. However, the uncertainty in the selection of the segmentation threshold directly affects the fracture extraction results. Julge et al. [18] applied it to the UAV image classification experiment and achieved 83% global accuracy and 77.36% Kappa accuracy. The classification results are highly consistent with the reference data type; in order to improve the extraction accuracy of ground fissures, the hit-to-hit transform algorithm connects the broken ground fissures, and at the same time, the small pattern removal algorithm combining shape and area proposed in this article is used to realize the removal of ground fissures and combined with ground fissure extraction results to conduct experiments to verify the effect of ground fissure fine treatment.

Zhang et al. [19] studied a fault-tolerant path planning algorithm, using multisensor fusion to study fault-tolerant path planning and using wireless communication systems for positioning. Basir et al. [20] studied the path planning algorithm based on a firefly under an uncertain environment, using the attraction law between fireflies to reduce the number of iterations and helping the robot to search for the optimal path in the constantly changing dynamic environment according to the local static environment. At the same time, a linear computational complexity graph search algorithm is proposed, which uses the priority queue, graph search, and the combination of a cattle to study a two-way sublist path planning algorithm that is faster than the

algorithm under global information. Domestic researchers have also made a lot of contributions in the field of path planning. Scholars have studied the PRM path planning algorithm based on distance transformation and constructed a narrow channel undirected graph based on image processing and random icon technology to study the density of obstacles [21–23]. The researcher proposed a multithreaded SA∗ path planning algorithm, adding multithreaded parallel computing to the A-Xing algorithm and using heuristic search to improve the SA∗ algorithm to improve the speed and accuracy of path calculation. Some scholars try to use the genetic iterative algorithm to extract road cracks, but the selection of the best parameters in the algorithm is still a problem worthy of in-depth study. In order to extract the cracks of concrete bricks, multiple threshold segmentation algorithms are used for experiments, although the final result is optimized to the subpixel level, but the threshold segmentation algorithm cannot distinguish targets with similar gray values, resulting in a large amount of background noise; in order to realize the automatic detection of cracks in concrete pipes, the researchers proposed a method to segment pipe images based on morphological methods [24–26].

3. Analysis of Landslide Monitoring System

3.1. Structural Diseases of Landslides. In the landslide structure, the broken rock mass of the slope top and the slope surface is the broken rock mass formed by the fracture and disintegration of the rock mass located on the top of the slope and the slope surface. At the initial stage of the formation of a landslide, the redistribution of stress resulted in the concentration of tensile stress on the top of the slope, pressure cracking on the slope, the development of tension and cracks in the rock mass, and the fragmentation of the rock mass. Collapse is a phenomenon in which the rock and soil on a high and steep landslide suddenly completely separates from the parent body under the action of gravity and external force, and then rolls, jumps, dumps or falls, and accumulates to the foot of the slope or the road:

$$\lim_{x\longrightarrow\infty} u_q(t,x) - \lim_{x\longrightarrow\infty} u_q(wxt+q)U = 0. \tag{1}$$

When the quaternion is updated, the Euler angle can be used to obtain the attitude angle in the dispatch, but the yaw angle is not used as the final yaw angle of the attitude, and it needs to go through the first-order complementary calculation. In the calculation, the complementary gyroscope calculated output specific gravity is increased, while the magnetometer output specific gravity is decreased, and the yaw angle is obtained by the fusion calculation:

$$\lim_{x\longrightarrow\infty} u_d(x,t) = \lim_{x\longrightarrow\infty} u_d(wxt-d)U. \tag{2}$$

The protective structure is a force-bearing structure set on the landslide slope surface to support the rock and soil pressure. The protective structure is mainly affected by water erosion and rock and soil pressure. The coagulation structure has a large amount of cement. The internal cracks in the concrete are the primary breakthrough points for water erosion. In these locations, the concrete is easy to peel off and the steel bars are exposed, causing structural damage and loss of function:

$$\lim_{x\longrightarrow\infty} u_d(\cos x,\ \sin x) = \lim_{x\longrightarrow\infty} \tan(xt-d)U. \tag{3}$$

The protective structure is mainly subjected to rock and soil pressure. When the local structural strength is lower than the structural stress, the structure will bend and fail. The magnetometer is susceptible to external interference when the drone is autonomously navigating. Therefore, the magnetometer data are not used during complementary fusion, but the value is the magnetometer output when the system initializes the quaternion:

$$\begin{bmatrix} u_d \\ u_q \end{bmatrix} \times \begin{bmatrix} u_d & u_q \end{bmatrix} = \begin{bmatrix} 1 & -1 \\ 1 & 1 \end{bmatrix} \times \begin{bmatrix} -u_d \\ u_q \end{bmatrix}. \tag{4}$$

In the safety judgment module, according to the drone landslide inspection results, the four aspects of landslide weathering degree, drainage system, protective structure, and other landslide phenomena are evaluated, and the corresponding options are selected in the inspection management system, such as weathering less intense, less intense, more intense, and intense. The inspectors make choices based on the actual inspection results. The system integrates these four options to determine the safety of the road landslide. The judgment results are as follows: stable, basically stable, understable, and unstable. After the judgment, the corresponding recommended treatment measures are displayed.

3.2. Classification of Landslide Safety Index. The landslide safety index information needs to be properly preserved. In the information management module, the information has been stored in the database. Users can export landslide information and inspection results to files by generating reports, which is convenient for users to save and can effectively ensure the safety of landslide data. In the safety prewarning module, users can also send the results of landslide inspection and treatment suggestions to managers' mailboxes to realize real-time communication and feedback functions:

$$F(s,t,\theta) = \begin{bmatrix} \sin\theta' & \cot\theta \\ \cot\theta' & \sin\theta \end{bmatrix} \times \begin{bmatrix} 1-u_s \\ 1-u_t \end{bmatrix}. \tag{5}$$

Finding the extreme point (gradient position) in the first-order derivative function of the gray value is a troublesome task, while finding the position where the second-order derivative function value is 0 is relatively easy. The second-order edge detection algorithm is to detect the pixel position in the image where the second-order derivative function value of the gray value is 0, which is regarded as an edge. Similar to the first-order derivative function, the second-order derivative function can be replaced by the second-order difference form of pixel gray value.

Under the premise of ensuring accuracy, the use of drone camera measurement technology can be used to monitor the deformation of the landslide group. For areas with a very

large number of landslides in Table 1, the deformation area has been monitored, and the identification of potential landslide areas has also been realized:

$$\prod f(x,t) \times U_i(s) - \prod f(x-1,t-1) \times \frac{s(s+w)}{w^2 - s^2} U = 0. \tag{6}$$

The above system errors have destroyed the central projection relationship between the objects, and the influence of the curvature of the Earth belongs to the difference caused by different projection transformations. The geoid is an ellipsoid. The ground coordinate system used in map projection uses a plane as a horizontal plane. When the aerial photography range is large, this difference will affect the accuracy of the aerial three encryption results, so it needs to be corrected. In the length of the buffer number of NS, the historical value of the appropriate interval is taken as the estimated value of the current moment according to the delay time of the auxiliary sensor:

$$\sum s(s+w) \times \sum w^2 - s^2 - \sum f(s,t) \times \frac{s(s+w)}{w^2 - s^2} = 0. \tag{7}$$

If it is under high-speed operation, the delay correction needs to use the least square fitting; that is, the delay correction buffer (effective broadband autonomous control algorithm value) is polynomial fitting, and the curve is fitted according to the buffer area. Then, use the median value average recursive filtering to calculate the optimal estimated value at the next moment, and refresh the buffer area.

In the same way, through the working principle of each module, the data manual can calculate that the maximum sampling frequency of ultrasound in this study is 75 ms, the maximum sampling frequency of GPS M8N is 100 ms, the maximum sampling frequency of the barometer is 20 ms, and the maximum sampling frequency of the optical flowmeter is 8 ms. The previous surveying and mapping scheduling, serial port receiving buffer, digital filtering, etc. will also have a period of time.

3.3. UAV Fine Inspection. The development of UAV fine remote sensing and photogrammetry science has enabled humans to use low-altitude, high-altitude, and even outer space sensors to obtain various image data reflecting the characteristics of the surface. By extracting the physical characteristics and information of various target objects, the spatial shape, location, nature, change, and the relationship with the environment are studied. Feature points are pixels that describe the geographic location of the same information in two or more images and are used for image geometric transformation, image splicing, and three-dimensional model generation:

$$\lim_{\theta \longrightarrow \infty} \Delta\theta - \left|\theta - 2\theta'\right| - \left|wt - 2\theta'\right| = 0. \tag{8}$$

The extraction of feature points is an important step in the processing of oblique photogrammetry. The relationship in Figure 1 between multiview images is constructed by conjugate points. At present, the photogrammetry community has proposed many methods for automatic extraction of connection points. Commonly used automatic connection point extraction algorithms include scale-invariant feature transform (SIFT) and fast robust feature (SURF), Harris, MSER (the most stable extreme value region), and FAST (features from accelerated segment test) algorithms.

Table 1: Monitoring instructions for deformed areas.

Monitoring test	Partial deformed areas		
	Phase A	Phase B	Phase C
1	2.30	2.44	2.58
2	1.77	1.87	1.97
3	1.24	1.30	1.36
4	0.71	0.73	0.75
5	0.18	0.16	0.14
6	−0.35	−0.41	−0.47
7	−0.88	−0.98	−1.08
8	−1.41	−1.55	−1.69
9	−1.94	−2.12	−2.30

In the actual field operation of tilt photogrammetry, the image will inevitably be affected by uncertain external factors, such as radiation distortion and geometric distortion in the image. For external influence factors, these operators can accurately extract feature points according to their respective characteristics and appropriate measures to extract feature points, and make the feature points have good uniqueness, antirotation, antiscaling, and antilight variation. For the matched connection points, the quality of these connection points has a greater impact on the later feature matching, which is directly related to its accuracy and accuracy:

$$\begin{cases} \lim\limits_{\theta \longrightarrow \infty} \sin\theta \times \cos\theta = \left|\theta - 2x'\right|, \\ \lim\limits_{\theta \longrightarrow \infty} \cos\theta \times \cos\theta = \left|\theta + 2x'\right|. \end{cases} \tag{9}$$

The monitoring personnel set the route and UAV parameters in the ground control system, and the aerial part of the UAV then performs the flight mission according to the instructions of the ground control system. UAV flight data are transmitted to the ground control system in real time using wireless transmission channels, and ground monitoring personnel can change the flight plan or let the UAV continue to execute instructions based on the received data. When you take supplementary shots of poorly-photographed areas, emergency situations, and landing, you can switch the flight status from automatic to manual control:

$$\left\langle \begin{matrix} u_\alpha(t) - u_\alpha(t-1) \\ u_\alpha(t) + u_\alpha(t-1) \end{matrix} \middle| \begin{matrix} \sin(wt) \\ \sin(w(t-1)) \end{matrix} \right\rangle = 1. \tag{10}$$

On the basis of network socket communication, the TCP or UDP protocol needs to be added. This study takes network communication based on the TCP protocol as an example. This protocol mainly uses the TcpClient and TcpListener classes built on socket. The attributes of the TcpClient class mainly include Available, ReceiveBufferSize, Client, Connected, LingerState, NoDelay, SendTimeout, etc. The TcpListener class is mainly used to monitor and receive incoming connection requests. It mainly includes five stages:

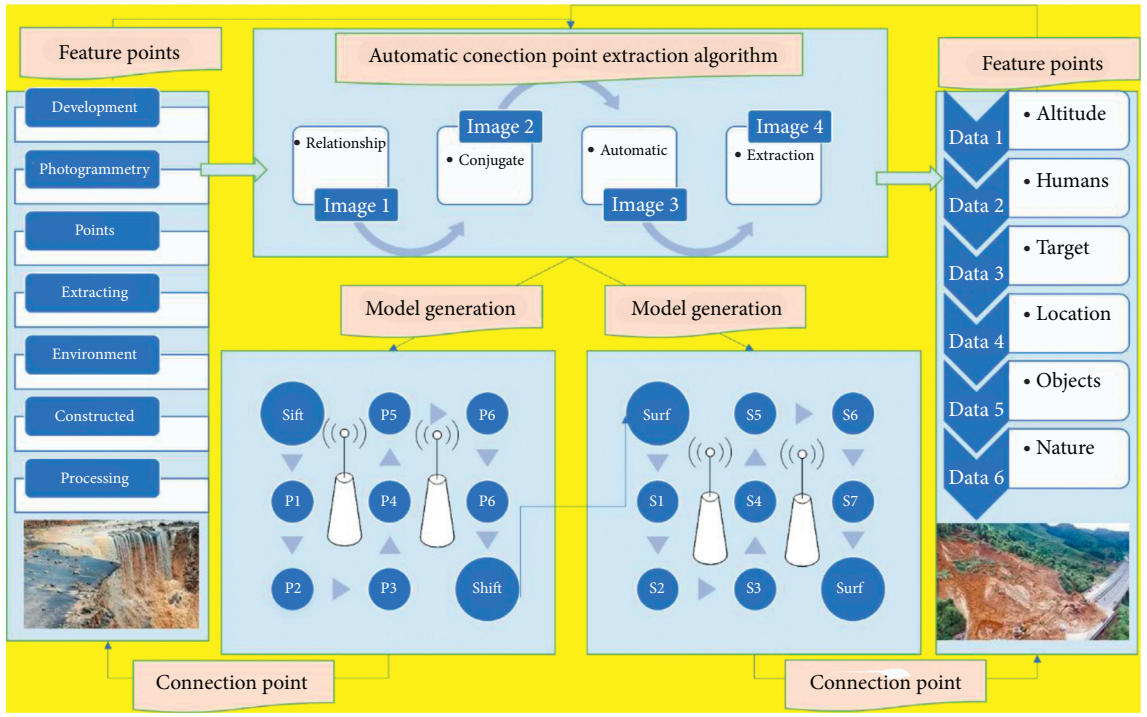

Figure 1: UAV fine inspection topology.

creating TCP instances, monitoring connections, receiving connection requests, sending and receiving data, and stopping services.

3.4. Image Processing Technology. The low-altitude UAV photogrammetry technology is mainly used for small surveys or emergency survey missions. It is characterized by unmanned aircraft as a flying platform, various types of sensors are used to obtain ground information, and computer graphics are used. Image technology processes the acquired images and provides basic data for various types of photogrammetry applications.

The data processing part includes a data preprocessing system and a data postprocessing system. The data preprocessing system includes photogrammetric data download, flight quality and data quality inspection, camera calibration, and distortion correction; data postprocessing includes air three processing, drawing production, interpretation, and result evaluation:

$$\int [u_\alpha(t) - \sin(wt) + \sin(w(t+1))]\mathrm{d}t = 0. \tag{11}$$

The UAV low-altitude photogrammetry system in Table 2 consists of two parts: data acquisition and data processing. Data acquisition refers to the route planning function of ground personnel through the ground monitoring system or the remote control card control system of the UAV remote control. We realize the take-off and landing of the UAV, and achieve the precise control of the drone dagger platform. Ground fissures are a form of existence of fissures on the ground, and their spatial form is characterized by dark tones and strip-like linear features.

The edge detection algorithm in computer vision is one of the earliest methods used for linear target extraction, which is mainly divided into the first-order edge detection algorithm and the second-order edge detection algorithm. The area where the local gray value changes obviously in the image can be regarded as the edge, and the change in the local gray value can be expressed by the first-order derivative function. If the value of the first derivative function is larger, the probability of becoming an edge is higher.

From a qualitative point of view, the deformation shown by the monitoring data and the orthographic image is basically the same as the difference result; from a quantitative point of view, there is a certain difference between the amount of deformation displayed by the difference model and the actual amount of deformation:

$$\left\langle \begin{array}{l} \sin(wt) + \sin[w(t+1)] = 0 \\ \cos(wt) - \cos[w(t+1)] = 0 \end{array} \right\rangle. \tag{12}$$

The amount of data in the same area has greatly increased, and the increase in the number of lenses has increased the amount of data, which brings a burden to subsequent image processing, and puts forward higher requirements on computer performance. The clustered multi-CPU and multi-GPU architecture is now used to handle tilt massive data obtained from photography. When the flight control board is rotated, the 3D modeling icon of the anonymous host computer will also rotate and the data will also change. It can be judged whether the IMU module can communicate normally according to the consistency of the rotation direction and the beating amplitude of the data change:

Table 2: UAV low-altitude photometric system.

Features step algorithm		Connection point 1	Connection point 2	Connection point 3	Connection point 4
Algorithm accuracy	SIFT 1	2.37	0.47	0.57	2.67
	SIFT 2	1.60	0.66	0.72	1.78
	SURF 1	0.83	0.85	0.87	0.89
	SURF 2	0.06	0.04	0.02	0.00
	MSER 1	−0.71	−0.77	−0.83	−0.89
	MSER 2	−1.48	−1.58	−1.68	−1.78

$$\text{if } (\sin t > \cos t), \text{c.t.out } f\left(x, t | x^2 + t^2 = 0\right) = \frac{\partial \sin(wt)}{\partial w \partial t}. \tag{13}$$

The low-altitude indoor autonomous control module, which is a combination of ultrasonic and optical flow meter, is connected to the reserved UART port of the flight control system. You can use the serial debugging assistant to check whether the data output is normal or the onboard OLED screen on the flight control system to observe the data.

4. UAV Surveying and Mapping Trajectory Scheduling and Autonomous Control Model Construction for Landslide Monitoring

4.1. UAV Mapping Trajectory Scheduling. The cameras carried by UAV photogrammetry are all nonmeasurement cameras, and the images acquired by them have a certain degree of distortion due to the time difference. The image must be removed before data processing. Through the adjustment of the position of the principal point of the image and the correction of the distortion parameters, the processing of the distortion effect on the image is realized.

In order to improve the matching speed of the image points with the same name and increase the density and accuracy of the matching points, it is necessary to create a pyramid for the image and perform image matching based on the image classification matching strategy that is gradually refined by the image pyramid, so that good reliability and high accuracy can be obtained to extract similar feature points from two adjacent images with a certain degree of overlap in Figure 2, and then use gray-scale or feature-based matching algorithms to match points with the same name, and obtain a point set after relative orientation.

The data transmission system consists of a modem and a radio station. The reference station modem encodes and modulates the relevant data, and then, the radio station transmits it. The radio station on the rover station receives and demodulates the relevant signal through the radio station. Finally, the three-dimensional coordinates of the point are calculated and processed by the real-time dynamic measurement software system.

In order to make up for the lack of edge extraction accuracy caused by the randomness of the threshold selection in the first-order edge detection algorithm, the second-order edge detection algorithm was proposed to search for the maximum point of the local gradient value of the first-order derivative function (i.e., the value of the first-order derivative function):

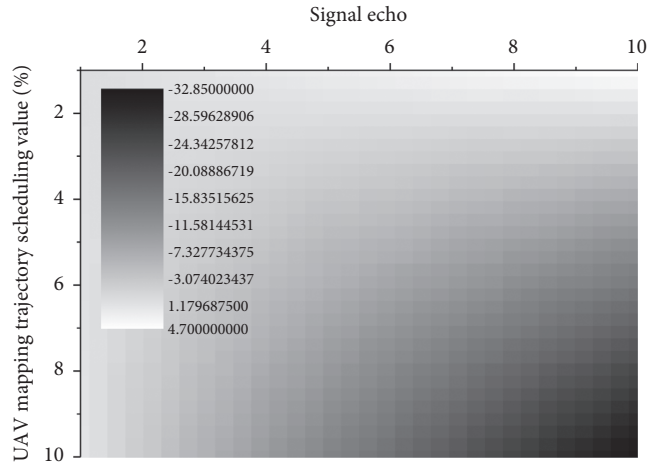

Figure 2: UAV surveying and mapping trajectory scheduling distribution.

$$\frac{\partial \sin(wt)}{\partial(wt)} + \frac{\partial \sin(w(t+1))}{\partial \cos(wt)} = 1, \quad \text{if } \{\cos(wt) - 1 < 0\}. \tag{14}$$

However, the analog image taken by a traditional film camera (i.e., an image with continuous image point and gray distribution) or a digital camera equipped with a charge-coupled device (CCD) is limited by the storage of digital devices such as computers. The captured digital image (i.e., the image in which the image point and gray-scale distribution are expressed in the form of discrete data), to be processed in the computer, must be stored in the form of discrete data.

4.2. Composition of Landslide Inspection Management System. The landslide inspection management system is divided into two parts: air and ground. The air part contains electronic equipment for sending data, external antennas, and ports for receiving data, while the ground part contains electronic equipment for sending data and various antenna interfaces. These are used for data transmission between air cruise control equipment and ground observation stations.

This part of the system contains equipment that enables the aircraft to take off and land. The launch system provides guarantee for the accelerated take-off of the UAV, and the recovery part provides guarantee for the safe landing of the UAV. Ground support equipment for air flight includes support equipment during the transportation phase and equipment during filming.

The function of the transportation safety assurance equipment is to protect the shooting equipment and mission equipment from damage, while the shooting safety assurance equipment refers to the equipment that allows the drone to take pictures safely in the field. In actual research, the raw data of the accelerometer and gyroscope in Figure 3 can be sent to MATLAB for FFT change, and the spectrum graph near the throttle can be analyzed, so that the frequency range of noise can be observed, and the MATLAB filter design toolbox can be used to study the filter parameter design to determine various parameters of Butterworth low-pass filtering. While determining the order of the filter, consider that although the higher the order, the faster the stopband attenuation, the system phase delay will also increase:

$$[\![\frac{-b \pm \sqrt{b^2 - 4ac}}{2a} \cos t]\!] \underset{|\theta - 2\theta'|}{\rightleftharpoons} \tan(ab)\cos t. \tag{15}$$

After comparing the theory of tilt and vertical photography, and based on the high-precision aerial photography plan of vertical photography, that is, postdifferential technology and reasonable image control point layout, tilt photography uses its multiview data acquisition and multiview joint adjustment to compare the postdifferential.

In the application of technology and image control point program, the elevation accuracy of tilt photography data results was compared with that of vertical photography. It was found that the elevation accuracy of tilt photography was improved to a certain extent compared with that of vertical photography, which provided high-precision program support for subsidence monitoring of tilt photography.

Under the condition of the same degree of overlap, the basis can only be increased by increasing the heading CCD width or shortening the focal length. However, the shorter the photographic baseline B, the more automatic the matching points, the easier the image matching, and the higher the relative orientation accuracy. SPP extracts fixed-dimensional features from the input object image. First, the maximum pooling divides the image into 4 feature maps, each of which extracts features of the same dimension and then pools the image into 16 feature maps with consistent dimensions.

After receiving the survey task, it is necessary to first analyze the survey task and objectives in detail to determine the flight platform and photogrammetric sensor to be used, and then choose to carry out drone aerial photogrammetry work based on the geological and meteorological conditions of the survey area in Table 3. The best season and time are finally used as the basis for field reconnaissance and comprehensive analysis based on the previous geological work degree and other data.

Optimizing the flight plan can effectively reduce the number of invalid flights and time. Based on a comprehensive understanding of the location and area of the target area, full consideration should be given to flight efficiency, and the minimum number of routes to the target should be used under the condition of ensuring full coverage of the target area.

4.3. Autonomous Control of Safety Early Warning. Safety early warning needs to introduce the tilt aerial photography program into the subsidence area, obtain the two phases of ground drone tilt data corresponding to underground mining activities, and use the level to measure the two phases of ground observation station data; carry out the two phases of drone tilt data.

The empirical parameters of the mine are used to predict the sinking basins, and the sinking basins are predicted to form. The sinking basins obtained by tilt photography are quantitatively analyzed using the measured observation line data, and Table 4 is used to predict the sinking basins. Qualitative analysis was performed on the acquired subsidence basin.

Compared with the subsidence difference between the two phases of ground observations, the two subsidence values are basically controlled within 150 mm, and the median error is 102 mm. Although there is a certain gap in the monitoring of the 10 mm terrain subsidence with slight changes, the mining parameters of this type, the aerial survey monitoring method has high reliability.

In order to facilitate reading and identification, it is necessary to renumber the images acquired in all directions and modify the image names according to certain rules. Since the original image is being shot, there are effects such as uneven illumination and changes in the sun's altitude angle, and the oblique image has forward and back light conditions. A uniform color and uniform light processing can be performed during preprocessing to ensure the natural color transition of the image:

$$\begin{aligned} &\oiint |wt - 2\theta'||wt + 2\theta'| \mathrm{d}w\mathrm{d}t \\ &\quad - \oiint |wt - \theta'||wt + \theta'| \mathrm{d}w\mathrm{d}t = 0. \end{aligned} \tag{16}$$

After superimposing the predicted subsidence basin with the aerial photography subsidence basin, we can intuitively see that the areas with larger subsidence values in the aerial photography subsidence basin tend to be on the west side of the aerial photography subsidence basin and are basically the same as the subsidence center of the predicted subsidence basin. The operations such as cropping and scaling, which are easy to lose information on the original image, are removed and replaced by a spatial pyramid pooling layer on the convolutional features.

The coincidence reflects the accuracy of aerial photography of the sinking trend of the subsidence basin; in addition, it can be seen that the subsidence range obtained by drone aerial photography is more comprehensive and broad to reflect the area affected by the subsidence of the mining area, breaking the traditional monitoring methods that can only be from one line. Observational bottlenecks reflect the comprehensiveness of using aerial photography to monitor subsidence trends:

$$\sqrt{\lim_{\theta \longrightarrow \infty} \Delta\theta \lim_{\theta \longrightarrow \infty} \Delta 2\theta} + \sqrt{\cos a^2 + \cos b^2} = 0. \tag{17}$$

Therefore, this study adopts the second-order Butterworth low-pass filter. The original data of the accelerometer and the data changed by FFT are simulated in MATLAB, and

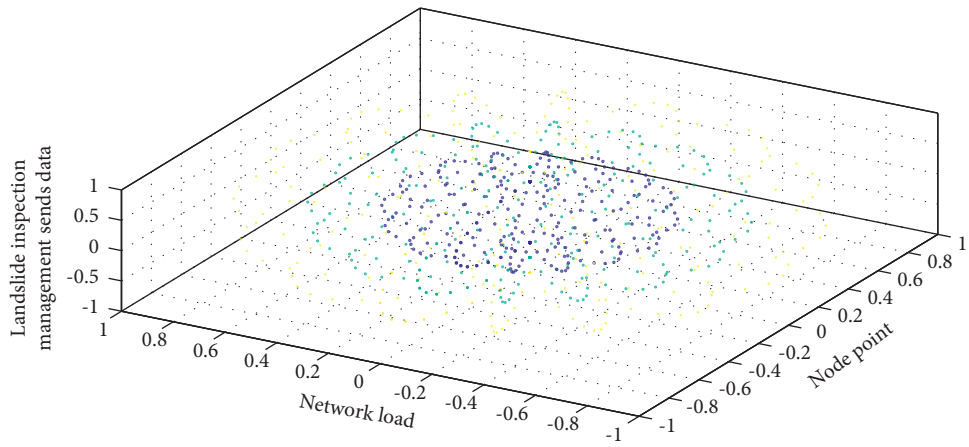

Figure 3: Distribution of data sent by landslide inspection management.

Table 3: Photogrammetric control algorithm of flight platform.

Steps number	Algorithm description	Code explanation
1	Autonomous navigation path $U_i(s)$	Int Index(char * S, char * T)
2	Vertical and oblique images $(n!/r!(n-r)!)$	B=(int *)malloc(sizeof(A));
3	The two phases of field $t-1$	Int $i=1,j=1$;
4	Its accuracy results $x-1$	While(i<=s[0]&&j<=T[0])
5	During the application process $\lim_{x\longrightarrow\infty}(n!/r!n!)$	//Merge(A,0,3,7);
6	Based on the Smart3D $\partial s \partial t$	If($S[i]==T[j]$){
7	Contextcapture platform $f(x,t)$	++i; ++j; }else
8	The point cloud of the survey area $\partial f(x,t)$	If($j==0\|\|S[i]==T[j]$){
9	UAV can directly carry out stable	{mergesort(A,0,7);
10	Drone tilt photogrammetry $U_i(s,t,x)$	I = i − j + 2; $j=1$;
11	Mages obtained by technology $i, j, k \in R$	Printf("%d ",$A[i]$); }
12	For the overall modeling of the target $F(a,b)$	If($j>T[0]$)return i-T[0];
13	UAV can directly carry out stable $\sum w^2 - s^2$	Else int next[], int pos
14	The host computer software $-b+\sqrt{b^2-4ac}$	Void get_nextone(char T[], int next[]){
15	Geometric center of the flight platform $\cos a$	While(i<=T[0])
16	The tilt angles of the pictures obtained $\cos b$	Int kmpone(char S[], char T[])
17	Object from multiple perspectives $R(\sin x, \cos s)$	While(i < S[0]&&j < T[0])

Table 4: Analysis of autonomous control of safety early warning.

Parameter name	Channel 1 subsidence value	Channel 2 subsidence value	Parameter requirements
Control method	19.31	47.37	External connection
Autonomous communication	19.62	47.74	Wireless communication
Warning bandwidth	19.65	47.77	500~1500 MHz
Control subsidence supply	19.25	47.30	Reserved for external interface
Control subsidence life	18.27	46.11	Continuous work conditions
Warning range	16.56	44.03	−40~−20 dbm
Analysis of channels	14.14	41.11	10

then, the accelerometer data after the second-order Butterworth filter with a cut-off frequency of 30HZ are simulated, and FFT simulation is performed. The processing results are as follows. We regard GCP coordinates as true values, image point coordinates (x, y) as observations, and image internal and external azimuth elements, various distortion parameters, and spatial coordinates of pending points as unknowns.

5. Application and Analysis of UAV Surveying and Mapping Trajectory Scheduling and Autonomous Control Model for Landslide Monitoring

5.1. Preprocessing of Landslide Monitoring Data. For the dangerous situation of landslide monitoring data, in addition to human operation errors, other situations can be avoided as much as possible. The DJI Phantom 4 Pro drone used in this article is equipped with front and rear obstacle avoidance functions, which can avoid hitting obstacles. In the case of weak GPS information, the drone will automatically hover and wait for a signal or return home automatically, which can avoid flight accidents.

On the basis of theoretical research, this article has done systematic software design and development of Beidou-based high-precision autonomous navigation and monitoring technology for UAVs. On the basis of self-made monitoring upper computer, self-made remote navigation communication system, and anonymous flight control system in Figure 4 UAV comprehensive test platform was built, and the software design of UAV high-precision positioning, UAV autonomous navigation inertial navigation algorithm, and UAV autonomous navigation path planning algorithm was completed. The bar is the b-box regression. As of now, the two network modes 1 and 2 do not share parameters, but are trained separately.

After the drone completes the aerial photography of the overall inspection, due to the drone's own image transmission function, the aerial image can be checked at the ground control station, and the landslide can be judged according to the method of visual interpretation. The image can be judged that the target landslide is within the image range. Then, check the quality of the image to see whether it is blurred or deformed. If such problems occur, it is generally caused by camera settings, lens contamination, high wind speed, etc. After the problem is resolved, we retake aerial photography or only re-shoot a part of the image:

$$\iiint \partial \frac{U_i(s,t,x)}{\partial s \partial t} + \frac{\partial f(x,t,s)}{\partial s \partial t} + \frac{\partial f(x,t)}{\partial s} = 1. \tag{18}$$

Aerial triangulation calculation is a critical step in UAV image processing. First, we use photogrammetry software to correct the distortion of the image acquired by the UAV, then perform air triple encryption, and use the results of air triple encryption to perform high-precision matching editing and acquisition. The DSM filter edit the DSM to get the DEM that filters the buildings, etc., and then, use the DEM to digitally differentiate and correct the image to obtain multiple digital orthoimages in units of frames, namely, the DOM, and finally stitch them into the final image data.

5.2. Realization of UAV Surveying and Mapping Trajectory Simulation. In order to realize the autonomous navigation and monitoring of UAVs, it is necessary to realize the technology of remote monitoring of UAVs by the host computer and remote binding tasks for UAVs online, so it needs to have the function of wireless communication. At the same time, a WIFI chip is added. If there is a WIFI signal in the surrounding environment, the host computer software of the monitoring system and the UAV can directly carry out stable and efficient two-way communication in the local area network:

$$\lim_{x \longrightarrow \infty} \frac{n!}{r!(n-r)!} - \lim_{x \longrightarrow \infty} \frac{n!}{r!n!} = 0, \quad \text{for}\{i, j, k \in R(\sin x, \cos s)\}. \tag{19}$$

Oblique photogrammetry carries cameras evenly distributed at different angles around the geometric center of the flight platform. There are two-lens oblique photography and five-lens oblique photography. The tilt angles of the pictures obtained by oblique photography are all greater than 3°, and the pictures obtained are called oblique pictures. Since oblique photography captures the target object from multiple perspectives, it is particularly advantageous for the interpretation of ground objects and targets, and has a higher quality assurance for the overall modeling of the target area:

$$\prod_{s.t.}^{a,c,t} F(a,b) * G(\cos a, \cos b) = \overbrace{\frac{-b+\sqrt{b^2-4ac}}{2a} * \cdots * \frac{-b-\sqrt{b^2-4ac}}{2a}}^{\text{for}\{a,b,c \in C\}}. \tag{20}$$

Aerial triangulation is the air three encryption. This is the most important link in the aerial photogrammetric image processing industry, and it is also a difficult point in the entire processing process. Its accuracy results directly affect the later digital elevation model DEM, digital ground model DSM, and digital positive. On the basis of datasets 1 and 2, it has been improved to form a new algorithm body model, which introduces a network structure instead of the selective search algorithm, and integrates the candidate frame generation into the deep neural network, which greatly simplifies the data set. The computational complexity and model complexity of 3, 4 improve the computational speed and the accuracy of the final result.

The dense point cloud is generated using the result of air three encryption, and the digital surface model data of the entire survey area are obtained. The digital surface model is filtered to remove some surface objects such as vegetation and then manually edited to obtain the digital elevation data that meets the requirements. Finally, it can be used to make 3D terrain of landslide.

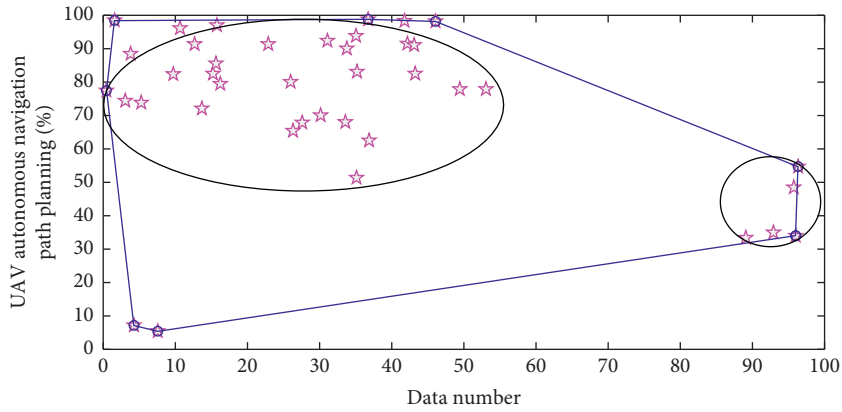

Figure 4: UAV autonomous navigation path planning.

The database is used to store the basic information of the landslide in Figure 5, such as the name of the landslide, lithology, topography, and rainfall, and it can also store the UAV landslide images and the results of the image post-processing. The rationality of database design is related to system calculation speed and accuracy. The research content of this article involves the import and export of a large amount of data. There are many types of stored data.

After the air triple encryption is completed, the DTM is extracted. The software calculates the radiation adjustment on a single image during processing to compensate for the visual effect and then adjusts the matching degree of adjacent images to balance the color of the image in the measurement area. The orthophoto map generated by the software can be exported to TIFF format and can be processed in ArcGIS software.

5.3. Case Application and Analysis. During the application process of the example, the point cloud of the survey area in this article is automatically processed based on the Smart3D ContextCapture platform, and the two phases of field vertical and oblique images obtained by drone tilt photogrammetry technology are combined with camera parameters and field image control points.

Using aerial triangulation technology to calculate the high-precision external orientation elements of each image, generate dense image points with the same name through dense matching, and then, perform matching after adjustment, until the matching points meet the accuracy requirements, and then, high-precision point clouds can be generated:

$$\begin{cases} u_\beta(t) = \cos(wt) + \exp(wt), \\ u_\beta(t-1) = \sin(wt) + \exp(wt), \\ u_\beta(t+1) = \tan(wt) + \exp(wt). \end{cases} \tag{21}$$

The 4G module uses the SIM7100 chip, which is an LTE platform based on Qualcomm's MHD9215 multiplexer. It has multiple frequency bands, including TDD-LTE//GSM/GNSS SMT. Its processor is provided by Cortex A5 (550HZ) and three QD SP6 (up to 500 MHz) built up. SIM7100 has powerful expansion functions, rich interfaces, including UART, SPI, and 12C, and flexible application capabilities, including TCP sampan DP/FTP. During hardware design, the module in Figure 6 is embedded in the navigation communication board and connected to the UART pin of STM32.

The point cloud generated by the tilted image of the drone contains a lot of noise and nonground points. This article processes the point cloud based on the 3D point cloud processing software and forms a high-precision point cloud after processing vegetation and high-voltage towers. Through this module, data can be sent to the WIFI network so as to realize the control and management of the Internet of Things.

The output candidate region of the first step of dataset mode 1 is used as the input of the detection network. A simple configuration before use can realize the networking function of the UART device. The SIM7100 is connected to the physical pin of the serial port 3 of the STM32, and the USR-C322 is connected to the physical pin of the serial port 2 of the STM32:

$$\left\langle \begin{matrix} R(\sin x,\ \cos s) \\ \sum f(s,t) \times \exp s \end{matrix} \middle| \left\langle \begin{matrix} -\langle (\partial f(x,t,s)/\partial s \partial t) \\ \sum f(s,t) \times \sin x \end{matrix} \right| = 0, \quad \text{for} \left\langle \begin{matrix} x > t \\ y < t \end{matrix} \right. \tag{22}$$

The landslide inspection management system needs to record and query the basic information of the landslide. In order to facilitate data entry, management, analysis, and query functions, corresponding data tables must be established to realize the above functions. A table is the most basic data storage unit of a database. It is a two-dimensional structure composed of rows and columns.

Columns are called fields and are used to define the structure of the table. Rows are called records and are used to store a piece of data in the table. We create corresponding fields in the table according to the characteristics of the data and set the appropriate data type for each field. In the landslide inspection management system, the types of data stored are different, and the fields in each table are also different.

According to Figure 7, the analysis of the results of the three sets of data under different image control point layout

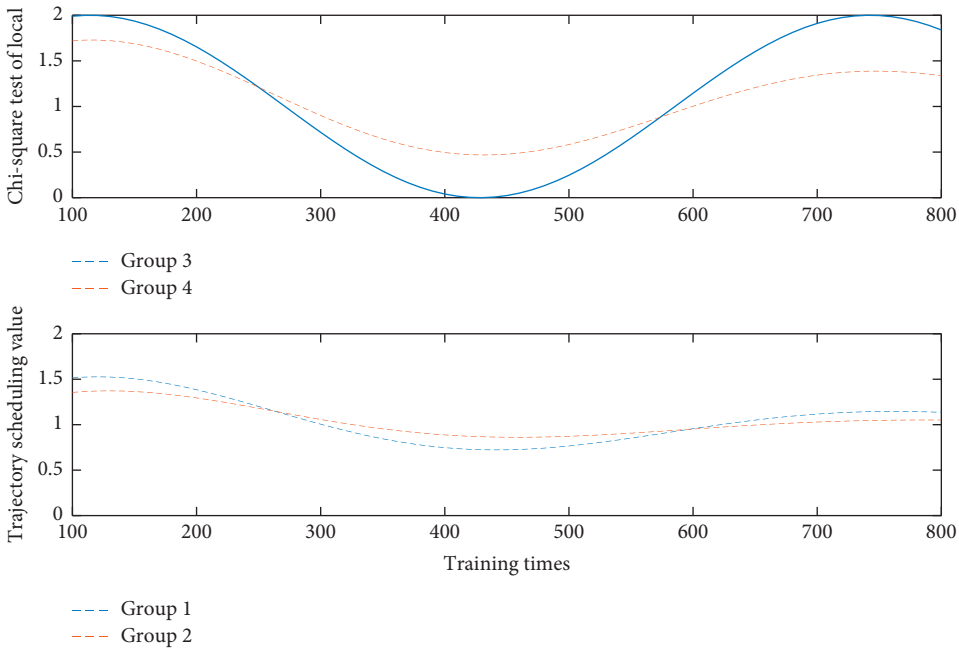

Figure 5: Dispatching distribution of 3D terrain trajectory of landslide.

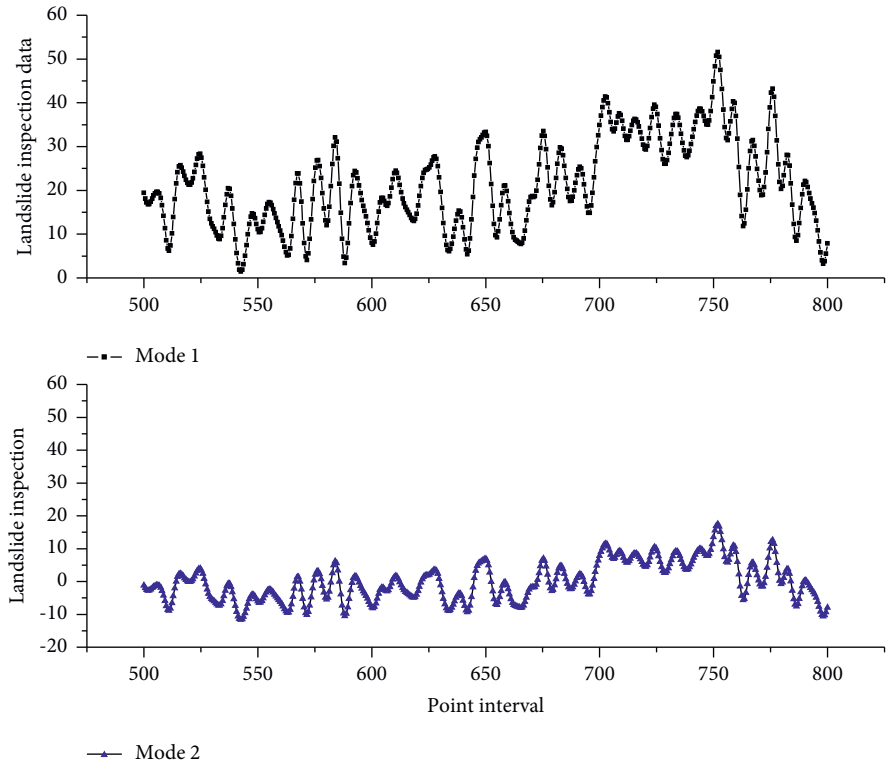

Figure 6: Data distribution of landslide inspection parameters.

schemes shows that the difference between the basic orientation point and the checkpoint of the data source I after using the differential technology is generally smaller than that of the data without using the differential technology. In terms of in-plane error, data source I is at least 2 times higher than data source II, and in elevation error accuracy, data source I can also be improved by more than 2 times compared to data source II.

The texture mapping based on the reconstructed TIN network mainly includes two parts: texture optimization and texture extraction. Due to the large overlap of the oblique images, most of the triangles reconstructed on the surface

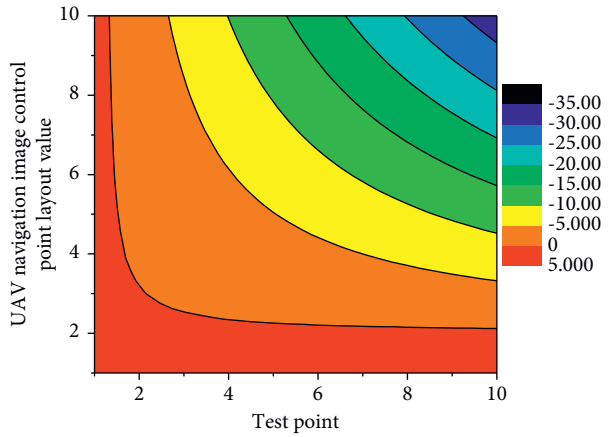

Figure 7: Layout of drone navigation image control points.

correspond to the corresponding textures of multiple images. The texture selection is based on the generated triangle mesh combined with the distortion parameters and the internal and external orientation elements of the image using photogrammetric computer vision methods:

$$\begin{Vmatrix} \cos t & -t \\ t & \sin t \end{Vmatrix} * \begin{Vmatrix} Ke^{-Kwt/2} & \tan t \\ -\tan t & -Ke^{-Kwt/2} \end{Vmatrix} = \begin{Vmatrix} \cos\left(1-K^2wt/2\right)U & 1 \\ 1 & \cos\left(1-K^2wt/2\right)U \end{Vmatrix}. \tag{23}$$

The monitoring data of the wooden piles showed that during the comparison time period, it shows a certain amount of deformation. The cumulative deformation of PM1 was 50 cm, and the cumulative deformation of PM2 was 4.4 cm. It can be seen that the trailing edge of the landslide is relatively broken and divided into pieces by cracks. Specifically, we output a candidate frame, intercept the original image through the candidate frame, pass the intercepted image through conVtool several times, and then output two branches through ROI-pooling, one for target classification and the other for target classification.

This is because the data source I adopts the post-difference technology, and the acquired image POS positioning information is processed by the difference software and the accurate latitude, longitude, and ellipsoid height at the time of camera exposure are calculated with higher accuracy, so the accuracy of the data source I will be higher than that of data source II; in addition, with the increase in the number of control points and the changes in positions, the error changes in the empty three planes have not changed significantly. This is because the nine points of the image control point scheme 1 are already available in this survey area. The plane accuracy is controlled to a higher level, but the error in the elevation is significantly improved, and the minimum is increased to more than 2 times.

6. Conclusion

This article studies the principle of landslide monitoring technology, and its double-difference positioning model introduces the core technology of UAV repair and detection and solving the ambiguity of the whole week, and derives the theoretical formula for the calculation of virtual observations and the establishment of the double-difference model. First of all, related software development is carried out on the network landslide monitoring technology, and the network landslide monitoring is applied to the positioning of the UAV. Secondly, it studied in detail the UAV surveying and mapping scheduling method based on complementary filtering, including Butterworth low-pass filtering technology and accelerometer gyroscope complementary filtering technology. On the basis of surveying and mapping scheduling, the vertical third-order complementary autonomous control algorithm with observer delay correction and the horizontal dual-observation autonomous control algorithm are studied, and simulations have verified the practicability. After that, according to the geometric attribute information of the ground fissures in the UAV image, the MF template and FDOG template that meet the vertical profile curve are constructed, and the UAV image is filtered and calculated separately to achieve the purpose of enhancing the ground fissure signal, and linear stretching is adopted. The method eliminates the difference in the value range obtained by the filtering operation and performs the difference operation between the two results to highlight the ground fissure signal in the image and weaken the edge signal of the ground feature. Finally, on the basis of autonomous control, the path planning algorithm is studied and the feasibility of the algorithm is verified by simulation, so that the UAV can avoid obstacles and complete the landslide monitoring task according to the optimal path under certain conditions.

Data Availability

The data used to support the findings of this study are available from the corresponding author upon request.

Conflicts of Interest

The authors declare that there are no conflicts of interest in this article.

Acknowledgments

This study was supported by "The Special Fund Construction Project of Superior Subject in Shaanxi Province colleges and universities (Grant no. 0602)."

References

[1] S. Aggarwal and N. Kumar, "Path planning techniques for unmanned aerial vehicles: a review, solutions, and challenges," *Computer Communications*, vol. 149, pp. 270–299, 2020.

[2] L. Patané, "Bio-inspired robotic solutions for landslide monitoring," *Energies*, vol. 12, no. 7, p. 1256, 2019.

[3] M. Erdelj, M. Król, and E. Natalizio, "Wireless sensor networks and multi-UAV systems for natural disaster management," *Computer Networks*, vol. 124, pp. 72–86, 2017.

[4] D. Giordan, M. S. Adams, I. Aicardi et al., "The use of unmanned aerial vehicles (UAVs) for engineering geology applications," *Bulletin of Engineering Geology and the Environment*, vol. 79, no. 7, pp. 3437–3481, 2020.

[5] P. Arena, F. D. Pietro, A. L. Noce, S. Taffara, and L. Patanè, "Assessment of navigation capabilities of mini cheetah robot for monitoring of landslide terrains," *Research and Technology for Society and Industry (RTSI)*, vol. 9, pp. 540–545, 2021.

[6] D. Mishra and E. Natalizio, "A survey on cellular-connected UAVs: design challenges, enabling 5G/B5G innovations, and experimental advancements," *Computer Networks*, vol. 182, Article ID 107451, 2020.

[7] C. Kyrkou, S. Timotheou, P. Kolios, T. Theocharides, and C. Panayiotou, "Drones: augmenting our quality of life," *IEEE Potentials*, vol. 38, no. 1, pp. 30–36, 2019.

[8] H. Hildmann and E. Kovacs, "Review: using unmanned aerial vehicles (UAVs) as mobile sensing platforms (MSPs) for disaster response, civil security and public safety," *Drones*, vol. 3, no. 3, p. 59, 2019.

[9] H. Wang, H. Zhao, J. Zhang, D. Ma, J. Li, and J. Wei, "Survey on unmanned aerial vehicle networks: a cyber physical system perspective," *IEEE Communications Surveys & Tutorials*, vol. 22, no. 2, pp. 1027–1070, 2019.

[10] J. Besada, L. Bergesio, I. Campaña et al., "Drone mission definition and implementation for automated infrastructure inspection using airborne sensors," *Sensors*, vol. 18, no. 4, p. 1170, 2018.

[11] M. Labbadi and M. Cherkaoui, "Robust adaptive backstepping fast terminal sliding mode controller for uncertain quadrotor UAV," *Aerospace Science and Technology*, vol. 93, Article ID 105306, 2019.

[12] K. O. Said, M. Onifade, J. M. Githiria et al., "On the application of drones: a progress report in mining operations," *International Journal of Mining, Reclamation and Environment*, vol. 35, no. 4, pp. 235–267, 2021.

[13] A. W. A. Hammad, B. B. F. da Costa, C. A. P. Soares, and A. N. Haddad, "The use of unmanned aerial vehicles for dynamic site layout planning in large-scale construction projects," *Buildings*, vol. 11, no. 12, p. 602, 2021.

[14] M. M. Eltabey, A. A. Mawgoud, and A. Abu-Talleb, "The autonomy evolution in unmanned aerial vehicle: theory, challenges and techniques," *Advances in Intelligent Systems and Computing*, pp. 527–536, 2020.

[15] A. Khan, S. Gupta, and S. K. Gupta, "Multi-hazard disaster studies: monitoring, detection, recovery, and management, based on emerging technologies and optimal techniques," *International Journal of Disaster Risk Reduction*, vol. 47, Article ID 101642, 2020.

[16] R. Zanol, F. Chiariotti, and A. Zanella, "Drone mapping through multi-agent reinforcement learning," *IEEE Wireless Communications and Networking Conference (WCNC)*, vol. 4, pp. 6-7, 2019.

[17] H. Valente de Figueiredo, O. Saotome, E. H. Shiguemori, P. Silva Filho, and V. V. Estrela, "Image database of low-altitude UAV flights with flight condition-logged for photogrammetry, remote sensing, and computer vision," *Imaging and Sensing for Unmanned Aircraft Systems: Volume 2: Deployment and Applications*, vol. 2, pp. 91–111, 2020.

[18] K. Julge, A. Ellmann, and R. Köök, "Unmanned aerial vehicle surveying for monitoring road construction earthworks," *The Baltic Journal of Road and Bridge Engineering*, vol. 14, no. 1, pp. 14–17, 2019.

[19] H. Zhang, E. Aldana-Jague, F. Clapuyt, F. Wilken, V. Vanacker, and K. Van Oost, "Evaluating the potential of post-processing kinematic (PPK) georeferencing for UAV-based structure- from-motion (SfM) photogrammetry and surface change detection," *Earth Surface Dynamics*, vol. 7, no. 3, pp. 807–827, 2019.

[20] R. Basir, S. Qaisar, M. Ali, N. Ahmad Chughtai, M. Ali Imran, and A. Hashmi, "Performance analysis of UAV-enabled disaster recovery networks," *Autonomous Airborne Wireless Networks*, pp. 157–194, 2021.

[21] Y. Sahraoui, C. A. Kerrache, M. Amadeo et al., "A cooperative crowdsensing system based on flying and ground vehicles to control respiratory viral disease outbreaks," *Ad Hoc Networks*, vol. 124, Article ID 102699, 2022.

[22] D. Hermle, M. Keuschnig, I. Hartmeyer, R. Delleske, and M. Krautblatter, "Timely prediction potential of landslide early warning systems with multispectral remote sensing: a conceptual approach tested in the Sattelkar, Austria," *Natural Hazards and Earth System Sciences*, vol. 21, no. 9, pp. 2753–2772, 2021.

[23] Á. Török, Á. Barsi, G. Bögöly, T. Lovas, Á. Somogyi, and P. Görög, "Slope stability and rockfall assessment of volcanic tuffs using RPAS with 2-D FEM slope modelling," *Natural Hazards and Earth System Sciences*, vol. 18, no. 2, pp. 583–597, 2018.

[24] I. Jeelani and M. Gheisari, "Safety challenges of UAV integration in construction: conceptual analysis and future research roadmap," *Safety Science*, vol. 144, Article ID 105473, 2021.

[25] S. Ekici, "Design of unmanned helicopter equipped with turboshaft engine for agriculture spraying mission based on thermodynamic analysis," *Journal of the Institute of Science and Technology*, vol. 10, no. 1, pp. 532–546, 2020.

[26] L. Tan, J. Guo, S. Mohanarajah, and K. Zhou, "Can we detect trends in natural disaster management with artificial intelligence? a review of modeling practices," *Natural Hazards*, vol. 107, no. 3, pp. 2389–2417, 2021.